2016

Dual Role of Sb Ions as Electron Traps and Hole Traps in Photorefractive Sn2P2S6 Crystals

B. E. Kananen

E. M. Golden

S. A. Basun

D. R. Evans

A. A. Grabar

See next page for additional authors

Authors

B. E. Kananen, E. M. Golden, S. A. Basun, D. R. Evans, A. A. Grabar, I. M. Stoika, J. W. McClory, N. C. Giles, and L. E. Halliburton

Research Article | Vol. 6, No. 12 | 1 Dec 2016 | OPTICAL MATERIALS EXPRESS 3992

Optical Materials EXPRESS

Dual role of Sb ions as electron traps and hole traps in photorefractive $Sn_2P_2S_6$ crystals

B. E. Kananen,[1] E. M. Golden,[1] S. A. Basun,[2,3] D. R. Evans,[2] A. A. Grabar,[4] I. M. Stoika,[4] J. W. McClory,[1] N. C. Giles,[1] and L. E. Halliburton[3,5*]

[1]*Department of Engineering Physics, Air Force Institute of Technology, Wright-Patterson Air Force Base, OH 45433, USA*
[2]*Air Force Research Laboratory, Materials and Manufacturing Directorate, Wright-Patterson Air Force Base, OH 45433, USA*
[3]*Azimuth Corporation, 4027 Colonel Glenn Highway, Suite 230, Beavercreek, OH 45431, USA*
[4]*Institute of Solid State Physics and Chemistry, Uzhgorod National University, 88 000 Uzhgorod, Ukraine*
[5]*Department of Physics and Astronomy, West Virginia University, Morgantown, WV 26506, USA*
**Larry.Halliburton@mail.wvu.edu*

Abstract: Doping photorefractive single crystals of $Sn_2P_2S_6$ with antimony introduces both electron and hole traps. In as-grown crystals, Sb^{3+} ($5s^2$) ions replace Sn^{2+} ions. These Sb^{3+} ions are either isolated (with no nearby perturbing defects) or they have a charge-compensating Sn^{2+} vacancy at a nearest-neighbor Sn site. When illuminated with 633 nm laser light, isolated Sb^{3+} ions trap electrons and become Sb^{2+} ($5s^25p^1$) ions. In contrast, Sb^{3+} ions with an adjacent Sn vacancy trap holes during illumination. The hole is primarily localized on the $(P_2S_6)^{4-}$ anionic unit next to the Sb^{3+} ion and Sn^{2+} vacancy. These trapped electrons and holes are thermally stable below ~200 K, and they are observed with electron paramagnetic resonance (EPR) at temperatures below 150 K. Resolved hyperfine interactions with ^{31}P, ^{121}Sb, and ^{123}Sb nuclei are used to establish the defect models.

OCIS codes: (160.5320) Photorefractive materials; (190.5330) Photorefractive optics; (160.2260) Ferroelectrics; (160.6000) Semiconductor materials; (300.6470) Spectroscopy, semiconductors.

References and links

1. S. G. Odoulov, A. N. Shumelyuk, U. Hellwig, R. A. Rupp, A. A. Grabar, and I. M. Stoyka, "Photorefraction in tin hypothiodiphosphate in the near infrared," J. Opt. Soc. Am. B **13**(10), 2352–2360 (1996).
2. A. A. Grabar, I. V. Kedyk, M. I. Gurzan, I. M. Stoika, A. A. Molnar, and Y. M. Vysochanskii, "Enhanced photorefractive properties of modified $Sn_2P_2S_6$," Opt. Commun. **188**(1–4), 187–194 (2001).
3. M. Jazbinšek, D. Haertle, G. Montemezzani, P. Günter, A. A. Grabar, I. M. Stoika, and Y. M. Vysochanskii, "Wavelength dependence of visible and near-infrared photorefraction and phase conjugation in $Sn_2P_2S_6$," J. Opt. Soc. Am. **22**(11), 2459–2467 (2005).
4. M. Imlau, V. Dieckmann, H. Badorreck, and A. Shumelyuk, "Tin hypothiodiphosphate: nonlinear response in the sub-100 fs time domain," Opt. Mater. Express **1**(5), 953–961 (2011).
5. Y. Skrypka, A. Shumelyuk, S. Odoulov, S. Basun, and D. Evans, "Light-induced absorption and optical sensitizing of $Sn_2P_2S_6$:Sb," Opt. Commun. **356**, 208–211 (2015).
6. A. Grabar, P. Mathey, and G. Gadret, "Manipulation of fast light using photorefractive beam fanning," J. Opt. Soc. Am. B **31**(5), 980–986 (2014).
7. P. Mathey, G. Gadret, A. Grabar, I. Stoika, and Y. Vysochanskii, "Photorefractive and photochromic effects in $Sn_2P_2S_6$ at various temperatures," Opt. Commun. **300**, 90–95 (2013).
8. A. Grabar, P. Mathey, and R. Iegorov, "Coherent semilinear oscillator with $Sn_2P_2S_6$:Sb crystals," Appl. Phys. B **105**(4), 813–819 (2011).
9. D. R. Evans, A. Shuymelyuk, G. Cook, and S. Odoulov, "Secondary photorefractive centers in $Sn_2P_2S_6$:Sb crystals," Opt. Lett. **36**(4), 454–456 (2011).
10. I. V. Kedyk, P. Mathey, G. Gadret, A. A. Grabar, K. V. Fedyo, I. M. Stoika, I. P. Prits, and Y. M. Vysochanskii, "Investigation of the dielectric, optical and photorefractive properties of Sb-doped $Sn_2P_2S_6$ crystals," Appl. Phys. B **92**(4), 549–554 (2008).
11. T. Bach, M. Jazbinšek, G. Montemezzani, P. Günter, A. A. Grabar, and Y. M. Vysochanskii, "Tailoring of infrared photorefractive properties of $Sn_2P_2S_6$ crystals by Te and Sb doping," J. Opt. Soc. Am. B **24**(7), 1535–

#279258 http://dx.doi.org/10.1364/OME.6.003992
Journal © 2016 Received 24 Oct 2016; revised 20 Nov 2016; accepted 22 Nov 2016; published 1 Dec 2016

Optical Materials EXPRESS

1541 (2007).
12. A. T. Brant, L. E. Halliburton, S. A. Basun, A. A. Grabar, S. G. Odoulov, A. Shumelyuk, N. C. Giles, and D. R. Evans, "Photoinduced EPR study of Sb^{2+} ions in photorefractive $Sn_2P_2S_6$ crystals," Phys. Rev. B **86**(13), 134109 (2012).
13. S. A. Basun, L. E. Halliburton, and D. R. Evans are preparing a manuscript entitled "Hyperbolic decay of photo-generated Sb^{2+} ions in $Sn_2P_2S_6$ crystals detected with a novel electron paramagnetic resonance technique."
14. E. M. Golden, S. A. Basun, D. R. Evans, A. A. Grabar, I. M. Stoica, N. C. Giles, and L. E. Halliburton, "Sn vacancies in photorefractive $Sn_2P_2S_6$ crystals: An electron paramagnetic resonance study of an optically active hole trap," J. Appl. Phys. **120**(13), 133101 (2016).
15. E. M. Golden, S. A. Basun, A. A. Grabar, I. M. Stoika, N. C. Giles, D. R. Evans, and L. E. Halliburton, "Sulfur vacancies in photorefractive $Sn_2P_2S_6$ crystals," J. Appl. Phys. **116**(24), 244107 (2014).
16. A. T. Brant, L. E. Halliburton, N. C. Giles, S. A. Basun, A. A. Grabar, and D. R. Evans, "Intrinsic small polarons (Sn^{3+} ions) in photorefractive $Sn_2P_2S_6$ crystals," J. Phys. Condens. Matter **25**(20), 205501 (2013).
17. G. Dittmar and H. Schäfer, "Crystal structure of $Sn_2P_2S_6$," Z. Naturforsch. C **29b**(5–6), 312–317 (1974).
18. K. Kuepper, B. Schneider, V. Caciuc, M. Neumann, A. V. Postnikov, A. Ruediger, A. A. Grabar, and Y. M. Vysochanskii, "Electronic structure of $Sn_2P_2S_6$," Phys. Rev. B **67**(11), 115101 (2003).
19. K. Glukhov, K. Fedyo, J. Banys, and Y. Vysochanskii, "Electronic structure and phase transition in ferroelectic $Sn_2P_2S_6$ crystal," Int. J. Mol. Sci. **13**(12), 14356–14384 (2012).

1. Introduction

Single crystals of $Sn_2P_2S_6$ (often referred to as SPS) have interesting and useful photorefractive properties [1–4]. Doping with antimony (Sb) ions has been shown to significantly improve the photorefractive response of the SPS crystals, especially in the 530-675 nm region [5–11]. Of special interest is the increase in the photorefractive sensitivity of Sb-doped SPS when there is a pre-exposure to light with wavelengths near the optical band edge [5,9]. Recent observations of the transmittance dynamics (i.e., temporal dependence) of a red testing beam after terminating an intense green "pre-illumination" beam suggest that at least two distinct primary traps with different thermal stabilities are present in the Sb-doped crystals [5]. To better understand these photoinduced results, the identification and characterization of all Sb-related optically active defects in SPS is needed.

In an SPS crystal, Sb^{3+} ($5s^2$) ions easily substitute for Sn^{2+} ($5s^2$) ions. These ions have the same electronic structure and similar ionic size (for sixfold coordination, the ionic radius of the Sb^{3+} and Sn^{2+} ions are 0.76 and 1.18 Å, respectively). In an otherwise stoichiometric as-grown crystal with no additional dopants present, Sn^{2+} vacancies are expected to provide charge compensation for the Sb^{3+} ions. Specifically, there will be one doubly ionized Sn^{2+} vacancy for every two Sb^{3+} ions, thus ensuring the overall neutrality of the crystal. These Sb^{3+} ions and Sn^{2+} vacancies may be well separated and thus act as isolated electron and hole traps, or they may thermally migrate to each other and form a close-associate pair (i.e., a donor-acceptor pair) that acts only as a hole trap. A recent electron paramagnetic resonance (EPR) study has shown that isolated Sb^{3+} ions trap an electron when an SPS crystal is illuminated at low temperature with light near the band edge [12]. The resulting Sb^{2+} ($5s^25p^1$) ions are stable for sample temperatures below approximately 200 K. Their thermal decay at higher temperatures is described by second-order kinetics with an activation energy of 420 meV [13]. Also, EPR has shown that isolated Sn^{2+} vacancies trap a hole during illumination at low temperatures [14]. Other defects in SPS identified by EPR include sulfur vacancies [15] and Sn^{3+} holelike small polarons [16].

We use EPR in the present paper to experimentally verify that the defect complex consisting of an Sb^{3+} ion and an adjacent doubly ionized Sn^{2+} vacancy serves as a hole trap in SPS crystals. The Sb^{3+} ion replaces a Sn^{2+} ion and has an effective charge of + 1 (relative to the regular lattice), whereas a doubly ionized Sn vacancy has an effective −2 charge. Before trapping the hole, this complex is a $(Sb\text{-}V_{Sn})^-$ defect with an effective −1 charge. After the hole is trapped, the complex becomes a neutral $(Sb\text{-}V_{Sn})^0$ defect. The trapped hole is localized primarily on the one $(P_2S_6)^{4-}$ unit that is adjacent to both the Sb^{3+} ion and the Sn vacancy. This anionic unit has a large negative charge and strongly attracts the hole. Resolved hyperfine interactions with ^{31}P, ^{121}Sb, and ^{123}Sb nuclei in the EPR spectra provide the key

Optical Materials EXPRESS

information that establishes the ground-state model of this Sb-related trapped hole center in SPS crystals.

2. Experimental details

The $Sn_2P_2S_6$ crystals have a monoclinic structure (space group *Pn* and point group *m*) below the paraelectric-ferroelectric phase change at 64 °C. At room temperature, the lattice constants are a = 9.378 Å, b = 7.488 Å, c = 6.513 Å, and β = 91.15°, with the b axis perpendicular to the mirror plane of the crystal [17]. The $(P_2S_6)^{4-}$ anionic groups exhibit strong covalent behavior and are separated by the more ionic Sn^{2+} ions [18].

A large single crystal of SPS with dimensions on the order of centimeters was grown by the vertical Bridgman method at Uzhgorod National University (Ukraine). A sample for our EPR experiments (2.0 × 2.5 × 2.5 mm^3) was then cut from this larger boule. Reference [14] describes details of the growth process. Starting materials ($Sn_{1.93}P_{2.03}S_{6.04}$) for this particular growth run were chosen to produce a Sn deficient crystal. Thus, a large concentration of Sn vacancies is present. Although not intentionally doped, this crystal also has a significant concentration of Sb impurities, most likely coming from the starting materials. In addition to Sn vacancies and Sb^{3+} impurities, sulfur vacancies are present in this as-grown Sn-deficient crystal.

A Bruker EMX spectrometer operating near 9.392 GHz was used to obtain the EPR spectra. The sample temperature was controlled in the 40-220 K region with an Oxford gas flow system. There were no EPR signals in the as-grown crystal at room temperature or at low temperature (when cooled in the dark), as the donors and acceptors are all in nonparamagnetic charge states with no unpaired spins. These defects are converted to paramagnetic charge states during exposure to 633 nm light from a He-Ne laser or 510 nm light from a Xe lamp while the sample is held at low temperature in the microwave cavity (the optical band edge of SPS is near 530 nm at room temperature and shifts to near 500 nm at lower temperature). The SPS crystal was glued to the polished bottom face of a 4 mm diameter and 24 cm long quartz rod inserted into the Oxford cryostat and microwave cavity (the sample and the lower 4 cm of the rod were in direct contact with flowing cold nitrogen or helium gas while the top of the rod remained at room temperature). During an optical illumination, light entering the polished top face of the rod (i.e., light pipe) was transmitted to the cold sample. The use of the quartz rod as a light guide led to uniform filling of the bottom face of the rod with light and to the loss of any polarization of the incident light. For illumination at 510 nm, the output of a 150 W ozone-free Xe arc lamp (Oriel Model 6255) was passed through a 510 nm band-pass interference filter with 10 nm bandwidth (Thorlabs FB510-10). Incident 510 nm light power at the top face of the quartz rod was 5 mW. For illumination at 633 nm, a cw He-Ne laser (Spectra-Physics Model 106-1) operating at a power level of 12 mW was used. Duration of exposures to the 510 or 633 nm light was typically 5 min (thus ensuring that the effects of the illumination on the defects had saturated).

3. Results

3.1 EPR spectra

Figure 1 shows the EPR spectrum obtained from an SPS crystal containing large concentrations of Sb ions and Sn vacancies. While being held at 42 K, the sample was initially exposed to 633 nm laser light. The light was then removed and the sample was warmed to 125 K and held at this temperature for 2 min to reduce interfering signals from isolated Sn and S vacancies [14,15]. These ramps up and down in temperature each took approximately 5 min. After returning to 42 K following this brief warming, the spectrum in Fig. 1 was taken with no further illumination.

Optical Materials EXPRESS

Two S = 1/2 Sb-related defects, with widely split hyperfine patterns, are identified in Fig. 1 by "stick" diagrams. Additional lines in the center region, between 322 and 345 mT, are from the remaining Sn and S vacancies. Isolated Sb^{2+} ions (trapped electrons) are indicated by the blue stick diagrams and $(Sb\text{-}V_{Sn})^0$ complexes (trapped holes) are indicated by the red stick diagrams. The large number of lines in each set are caused by the hyperfine interactions of the unpaired electron with the magnetic moments of the ^{121}Sb and ^{123}Sb nuclei (^{121}Sb nuclei are 57.3% abundant and their I = 5/2 nuclear spin gives six hyperfine lines whereas ^{123}Sb nuclei are 42.7% abundant and their I = 7/2 nuclear spin gives eight hyperfine lines). Nuclear magnetic moments for the Sb isotopes are $\mu(^{121}Sb) = +\ 3.3634\beta_n$ and $\mu(^{123}Sb) = +\ 2.5498\beta_n$ (where β_n is the nuclear magneton). The ^{121}Sb and ^{123}Sb hyperfine parameters for a specific defect are proportional to their respective μ/I values. The isolated Sb^{2+} set of EPR lines in Fig. 1 (blue stick diagrams) has been previously reported [12]. In the present paper, our focus is on the newly observed $(Sb\text{-}V_{Sn})^0$ trapped-hole defects.

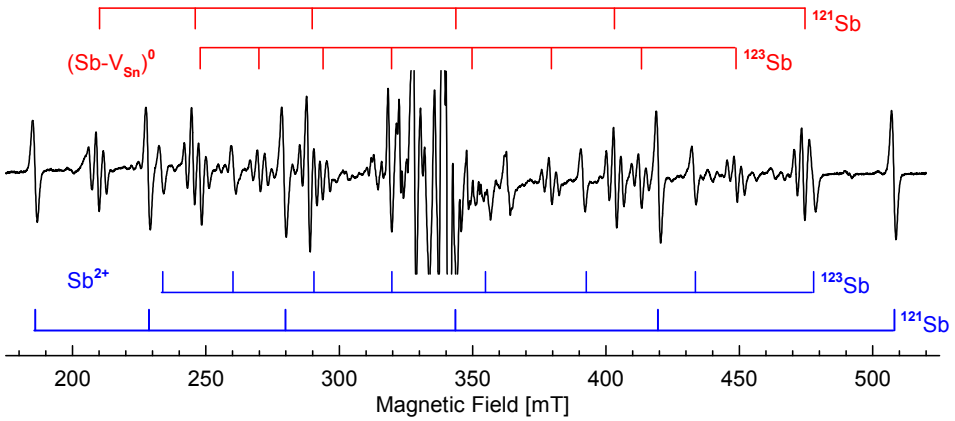

Fig. 1. EPR spectrum from an SPS crystal taken at 42 K with the magnetic field along the *a* axis. Blue stick diagrams identify lines from the Sb^{2+} ions (trapped electrons) and red stick diagrams identify lines from $(Sb\text{-}V_{Sn})^0$ complexes (trapped holes). Hyperfine lines from the ^{121}Sb and ^{123}Sb nuclei are present for both defects, as well as ^{31}P hyperfine triplets for the $(Sb\text{-}V_{Sn})^0$ complexes.

In Fig. 1, each Sb hyperfine line in the $(Sb\text{-}V_{Sn})^0$ spectrum (the red stick diagrams) is a set of three closely spaced lines with approximate intensity ratios of 1:2:1. These triplets are caused by nearly equal hyperfine interactions with two ^{31}P nuclei (the nuclear spin of ^{31}P is I = 1/2 and they are 100% abundant). The triplet sets of lines strongly suggest that the wave function for the unpaired spin has significant overlap with one $(P_2S_6)^{4-}$ anionic unit (and thus with its two ^{31}P nuclei), as well as the interaction with one Sb ion at a Sn site. The recent study of the EPR spectrum from singly ionized Sn vacancies in SPS shows similar hyperfine interactions with two ^{31}P nuclei [14]. Table 1 provides a comparison of the ^{31}P hyperfine interactions for the two trapped hole centers when the magnetic field is along the three crystallographic directions. For the $(Sb\text{-}V_{Sn})^0$ center, any difference in the strength of the interactions with the two ^{31}P nuclei is not resolved (i.e., the difference in these interactions is less than the linewidth). In the case of the isolated Sn vacancy, the two ^{31}P interactions are not equal in magnitude and vary by at most a factor of three [14]. Both defects have a Sn vacancy as the primary element in their models, thus it is not surprising that the trapped hole in each case has similar interactions with the two ^{31}P nuclei in the one adjacent $(P_2S_6)^{4-}$ unit and that the magnitudes of these ^{31}P interactions are comparable for the two defects. We take the values of the ^{31}P hyperfine interactions in Table 1 to be compelling evidence that the new $(Sb\text{-}V_{Sn})^0$ center consists of both a Sn vacancy and a localized hole, as well as the Sb ion. For

Optical Materials EXPRESS

perspective, hyperfine interactions with the two ^{31}P nuclei in the singly ionized sulfur vacancy are smaller, with magnitudes varying from 0.66 to 1.30 mT [15].

Table 1. Comparison of ^{31}P hyperfine interactions for the (Sb-V_{Sn})^0 trapped hole center and the isolated singly ionized Sn vacancy. Units are mT. For each defect, two ^{31}P nuclei in one (P_2S_6) unit are participating (they are arbitrarily labeled nucleus 1 and nucleus 2).

	Magnetic field direction		
	a	*b*	*c*
(Sb-V_{Sn})^0 trapped hole center[a]			
^{31}P hyperfine (nucleus 1)	2.81	3.38	2.85
^{31}P hyperfine (nucleus 2)	2.81	3.38	2.85
Isolated Sn vacancy[b]			
^{31}P hyperfine (nucleus 1)	3.02	3.41	2.91
^{31}P hyperfine (nucleus 2)	8.95	5.03	5.15

[a]Present study.

[b]From E. M. Golden *et al*., J. Appl. Phys. **120**, 133101 (2016).

An isothermal annealing study at 210 K was used to determine the stability of the (Sb-V_{Sn})^0 hole centers. The crystal was initially illuminated at 85 K with 510 nm light (obtained from a combined 150 W Xe lamp and band-pass filter). After removing the light, the intensities of the EPR spectra for the (Sb-V_{Sn})^0 and Sb^{2+} centers were recorded at 85 K. Then, with the sample still in the microwave cavity, the temperature was increased to 210 K and held there for 5 min, before returning to 85 K where the EPR spectra were recorded again. (Ramp rates up and down were 5 K/min.) This sequence was repeated for additional annealing times of 10, 15, and 30 min (the accumulated annealing time at 210 K was 60 min). This is similar to the process used in Reference [13] to determine activation energies. After 15 min of annealing at 210 K, 37% of the (Sb-V_{Sn})^0 signal remained and 92% of the Sb^{2+} signal remained. After 60 min of annealing, less than 20% of the (Sb-V_{Sn})^0 signal remained while 64% of the Sb^{2+} signal remained. Although both of the centers thermally decay at 210 K, the (Sb-V_{Sn})^0 hole centers are slightly less stable than the Sb^{2+} electron centers, and thus decay faster.

3.2 Spin-Hamiltonian parameters

The *g* matrix and the ^{121}Sb hyperfine matrix describing the (Sb-V_{Sn})^0 center were obtained from the angular dependence of the EPR spectrum (measurements were made in three planes). These results are presented in Table 2. Corresponding principal values for the ^{123}Sb hyperfine matrix can be extrapolated from the ^{121}Sb results using the known nuclear magnetic moments. Results for the Sb^{2+} electron center [12] are also included in Table 2. For the (Sb-V_{Sn})^0 center, the 12 × 12 matrix form of the spin Hamiltonian ($H = \beta \mathbf{S}\cdot\mathbf{g}\cdot\mathbf{B} + \mathbf{I}\cdot\mathbf{A}\cdot\mathbf{S}$) was repeatedly diagonalized in a least-squares fitting process as the **g** and **A** matrix parameters were varied. It is important to note that the ^{121}Sb hyperfine interactions are large and the hyperfine lines in the EPR spectrum are not equally spaced (see Fig. 1). Significant second-order shifts due to the large hyperfine principal values cause the spacing between adjacent Sb hyperfine lines to increase at higher magnetic field. In contrast, hyperfine interactions for the ^{31}P nuclei are smaller, and the values presented in Table 1 are taken directly from separations between lines in the EPR spectra.

Optical Materials EXPRESS

Table 2. Spin-Hamiltonian parameters for the $(Sb\text{-}V_{Sn})^0$ trapped hole center and the Sb^{2+} trapped electron center. Principal-axis directions are expressed as (θ,ϕ) pairs. The polar angle θ is defined relative to the *c* axis and the azimuthal angle ϕ is defined relative to the *a* axis with positive rotation from *a* toward *b* in the plane perpendicular to *c*.

principal values	principal axis directions θ	ϕ	principal values	principal axis directions θ	ϕ
$(Sb\text{-}V_{Sn})^0$ trapped hole center[a]			**Sb^{2+} trapped electron center**		
g matrix			*g* matrix		
1.850	91.4°	241.6°	1.810	68.7°	218.6°
1.888	125.1°	332.5°	1.868	49.6°	109.2°
1.925	35.1°	329.6°	1.887	48.0°	329.2°
^{121}Sb hyperfine matrix			^{121}Sb hyperfine matrix		
1153 MHz	117.0°	234.4°	1404 MHz	34.7°	213.0°
1473 MHz	86.6°	146.1°	1687 MHz	121.9°	187.3°
1679 MHz	152.8°	62.7°	1849 MHz	77.9°	104.9°

[a]Present study.

[b]From A. T. Brant *et al*., Phys. Rev. B **86**, 134109 (2012).

4. Discussion

As shown in several earlier investigations [7,10,11], the introduction of Sb^{3+} ions into SPS crystals is accompanied by a broad optical absorption appearing as a shoulder just below the optical band edge. In our sample, the peak of this poorly resolved optical absorption band is near 600 nm and its tail extends beyond 700 nm. The 510 nm light used in the present investigation is very close to the optical band edge. As expected, it transfers an electron from the valence band to the conduction band (at low temperature, the electrons and holes generated in this process are then trapped at the Sb-related donors and acceptors). Because 633 nm is well below the band edge, this light transfers an electron from the valence band to the Sb donor (without involving the conduction band). The hole left in the valence band is quickly trapped at the Sb-related acceptor. Thus, as we observe for 633 nm illumination at low temperature, this valence-band-to-donor transition leaves a trapped hole at the acceptor and a trapped electron at the donor.

Figures 2(a) and 2(b) show an isolated Sb^{3+} ion and an Sb^{3+} ion with an adjacent Sn vacancy, respectively. These schematic representations describe the Sb-related structures present in an SPS crystal before any illumination. The Sb^{3+} ions readily replace Sn^{2+} ions (the same bonding scheme is preserved because both ions have the $5s^2$ electron configuration). In the SPS crystal, the effective charge (relative to the regular unperturbed crystal) is different for these two Sb-related defects. During an illumination, the isolated Sb^{3+} ions in Fig. 2(a), with an effective charge of + 1, will trap photoinduced electrons whereas the $Sb\text{-}V_{Sn}$ centers in Fig. 2(b), with an effective charge of −1, will trap photoinduced holes. Prior to the present study, Sb was expected to act only as an electron trap in SPS [12]. Now, the possibility of forming defect complexes involving adjacent donors and acceptors allows a donor such as Sb^{3+} to be part of a hole trap.

Optical Materials EXPRESS

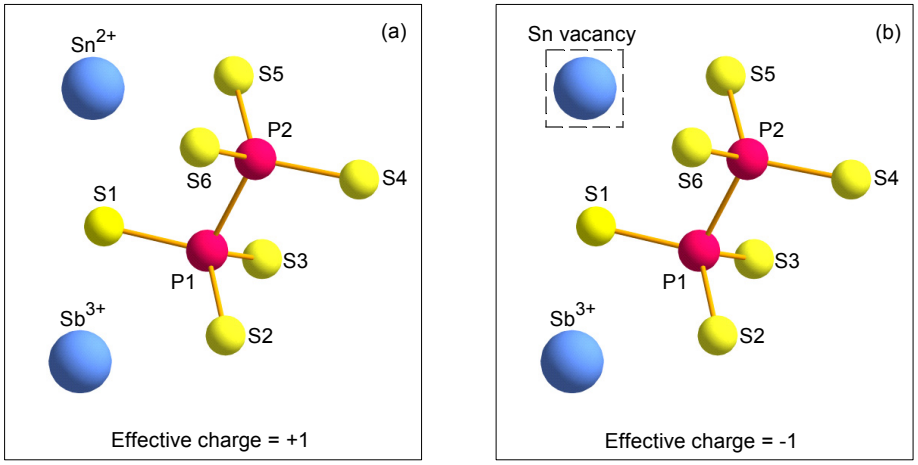

Fig. 2. Models of Sb-related defects in an SPS crystal (before illumination), (a) Isolated Sb^{3+} ion with no nearby defects. During illumination, this defect attracts an electron and forms a trapped-electron center. (b) Sb^{3+} ion with a neighboring Sn vacancy. During illumination, this complex attracts a hole and forms a trapped-hole center.

Our assignment of the new trapped-hole EPR spectrum in Fig. 1 (red stick diagram) to a Sn vacancy with an adjacent Sb^{3+} ion is based primarily on a comparison to the previously reported EPR spectrum from isolated singly ionized Sn vacancies [14]. These spectra have two features in common that provide support for this assignment. First, the two ^{31}P hyperfine interactions are similar for the two defects (see Table 1). Second, hyperfine interactions with the nucleus at the neighboring cation site are similar (a ^{117}Sn or ^{119}Sn nucleus for the isolated Sn vacancy and a ^{121}Sb or ^{123}Sb nucleus for the $(Sb\text{-}V_{Sn})^0$ center. This second common feature is especially important. Approximately 22.5% of the unpaired spin density was estimated to be on the adjacent Sn ion in the singly ionized Sn vacancy [14], and the parameters in Table 2 suggest that a similar amount of spin density is on the Sb ion in the $(Sb\text{-}V_{Sn})^0$ center [12]. For both of these Sn-vacancy-associated defects, the observed hyperfine interactions with the neighboring cation are a result of hybridized sp^2 (or sp^2d^5) combinations of S and Sn (or Sb) atomic orbitals [19]. More generally, there is hybridization between Sn (or Sb) atomic orbitals and P_2S_6 molecular orbitals. Future density-functional-theory (DFT) calculations will clarify the roles of covalency, electron lone pairs, and stereoactivity in the electronic structure of these holelike point defects, and also determine if the slightly smaller Sb^{3+} ion is displaced "off-center" at the Sn^{2+} site.

5. Summary

Electron paramagnetic resonance (EPR) is used to identify a new Sb-related defect in SPS. This defect consists of a charge compensating Sn vacancy next to a Sb^{3+} ion. During an illumination, this complex traps a hole and becomes EPR-active, i.e., a paramagnetic $(Sb\text{-}V_{Sn})^0$ center forms that is easily monitored at low temperature. Hyperfine structure in the spectra suggest strong similarities between the electronic ground state of the $(Sb\text{-}V_{Sn})^0$ center and the isolated singly ionized Sn vacancy [14]. When doping SPS with Sb, the relative concentrations of isolated Sb^{3+} ions and Sn-vacancy-associated Sb^{3+} ions may vary from crystal to crystal, depending on how many of the Sn vacancies (ranging from all to none) are located next to Sb^{3+} ions. Controlling factors include heating profiles during growth and possible post-growth heat treatments. Thus, not all Sb-doped SPS crystals are expected to have the same photorefractive response.

Optical Materials EXPRESS

Acknowledgments

Dr. John Luginsland at the Air Force Office of Scientific Research (AFOSR Project 16RT0053) supported the work at the Air Force Institute of Technology, and the Science and Technology Center in Ukraine and the European Office of Aerospace Research and Development (STCU/EOARD Project P438a) supported the work at Uzhgorod National University. Views expressed in this paper are those of the authors and do not necessarily reflect the official policy or position of the Air Force, the Department of Defense, or the United States Government.